Melt Electrovortex Flow in DC EAF Model with Two Bottom Electrodes in Axial Magnetic Field

Sergejs Pavlovs
Institute of Numerical Modelling
University of Latvia
Riga, Latvia
sergejs.pavlovs@lu. lv

Andris Jakovics
Institute of Numerical Modelling
University of Latvia
Riga, Latvia
andris.jakovics@lu.lv

Alexander Chudnovsky
JSC LATVO
Riga, Latvia
eivf19@gmail.com

***Abstract*—Paper presents computation results for molten steel flow in truncated cone bath in Electrical Arc Furnaces (EAF) of industrial scale. EVF is driven with direct electrical current (DC), supplied over arc spot at melt mirror and two bottom non-submerged electrodes. Several cases of time-averaged flow patterns, computed with large eddy simulation (LES) model of turbulence, are discussed: i) electrovortex flow (EVF); ii) melt rotation in external magnetic field; iii) influence of geomagnetic field on EVF.**

***Keywords—DC EAF, EVF, melt rotation, external magnetic field, geomagnetic field, LES study*.**

I. Introduction

The numerical research, concerned with LES-study of melt flow patterns in metallurgical MHD devices with combined power supply by inductor and over electrodes [1], is enhanced for computations taking into account external uniform magnetic field. The aim is the estimation of influence of external magnetic field on EVF in industrial scale DC EAF.

The computation approach is verified by comparison with measurements of magnetic field [2] and EVF velocity and flow patterns [2–4] in experimental setups with two cooper electrodes, fully submerged into cylindrical or rectangle bath with *GaInSn* or mercury melts.

II. Computational Model

A schematic of DC EAF computational model is shown in Fig. 1. Melt vessel geometry and melt parameters are provided in Table I. Electrodes geometry and parameters of conductive power supply are given in Table II. Industrial scale DC EAF equipment is chosen as the prototype for numerical model. Note, that similar model (bottom electrodes are not shifted from vertical symmetry plane) is considered in [5].

III. Peculiarities of Numerical Computations

Stationary magnetic field for multi-electrode models supplied with DC as well as *Lorentz* force in liquid metal (considering external magnetic field) was computed in *ANSYS Maxwell*.

Transient hydrodynamic (HD) field in the liquid metal was computed with *ANSYS FLUENT* using LES turbulence modelling. *Reynolds* number estimates with geometric and liquid metal parameters given in Table I and computed velocity values (Fig. 2 and 3) give $Re \sim 4.8 \cdot 10^5$.

Computational mesh for the HD field has ~3*M* elements with inflation at wall near bottom unsubmerged electrodes.

This work was funded by European Regional Development Fund under contract "Development of numerical modelling approaches to study complex multiphysical interactions in electromagnetic liquid metal technologies" (No. 1.1.1.1/18/A/108)

TABLE I. Geometric Parameters of the Melt Vessel and Melt Properties

Melt bath (truncated cone)	
Top (melt mirror) radius	$r_{melt}^{top} = 0.9\ m$
Bottom radius	$r_{melt}^{bottom} = 0.5\ m$
Height	$H_{melt} = 0.335\ m$
Molten steel	
Electrical conductivity	$\sigma_{melt} = 1.1 \cdot 10^6\ S/m$
Density	$\rho_{melt} = 6.9 \cdot 10^3\ \ kg/m^3$
Dynamic viscosity (laminar)	$\eta_{melt} = 6 \cdot 10^{-3}\ kg/(m \cdot s)$
Cinematic viscosity (laminar)	$\upsilon_{melt} = 8.7 \cdot 10^{-7}\ m^2/s$

TABLE II. Geometric Parameters of Electrodes and Supplied Direct Current

Top electrode	
Radius of arc spot at the melt mirror	$r_{el}^{top} = 0.14\ m$
Bottom electrodes	
Radius	$r_{el}^{bottom} = 0.0575\ m$
Distance between the axes of electrodes	$L_{el-el}^{bottom} = 0.6\ m$
Offset of the electrodes axes from symmetry plane	$L_{shift}^{bottom} = 0.1\ m$
Direct current (DC)	
Top electrode	$I_{el}^{top} = 40\ kA$
Bottom electrodes	$I_{el}^{bottom} = 20\ kA$

IV. Lorentz Force for EVF in External Magnetic Field

EVF in the melt is driven by *Lorentz* force $\boldsymbol{f}^{self}$, which is the result of interaction between electrical current $\boldsymbol{j}$ and self-magnetic field $\boldsymbol{B}^{self}$:

$$\boldsymbol{f}^{\text{self}} = \boldsymbol{j} \times \boldsymbol{B}^{\text{self}} \tag{1}$$

Electrical current $\boldsymbol{j}$ in melt interacts also with external uniform magnetic field. For chosen external magnetic field $\boldsymbol{B}^{ext}$ the contribution $\boldsymbol{f}^{ext}$ to *Lorentz* force is:

$$\boldsymbol{f}^{ext} = \boldsymbol{j} \times \boldsymbol{B}^{ext} \tag{2}$$

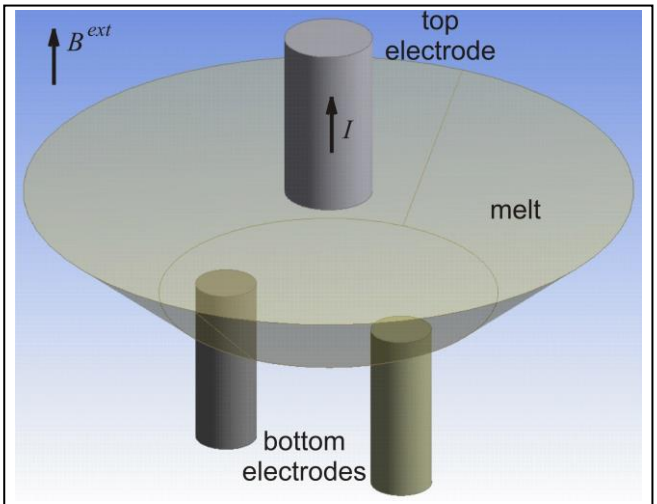

Fig. 1. Computational model of DC EAF

Total *Lorentz* force is:

$$\boldsymbol{f}^{total} = \boldsymbol{f}^{self} + \boldsymbol{f}^{ext} \quad (3)$$

Contribution of terms in formula (3) can be estimated by comparison of two non-dimensional numbers:

$$S = \frac{\mu_0 \left(I_{el}^{top}\right)^2 H_{melt}^3}{2\pi^2 \left(r_{el}^{top}\right)^3 \rho v^2}; N = \frac{I_{el}^{top} \cdot B^{ext} H_{melt}^3}{\pi \left(r_{el}^{top}\right)^2 \rho v^2} \quad (4)$$

where *S* is parameter of EVF and *N* is parameter of influence of external magnetic field.

V. Computational Results

Computational results for the melt flow driven by various distribution of the *Lorentz* force are presented in Fig. 2 and 3, and Table III.

TABLE III. Magnetic Field, Electrical Current and *Lorentz* Force in the Melt

Highest computed values in the melt	
Current density magnitude – $max\|\boldsymbol{j}\|$	$1.07 \cdot 10^6\ A/m^2$
Self-magnetic field magnitude – $max\|\boldsymbol{B}^{self}\|$	0.0581 T
External magnetic field $\boldsymbol{B}^{ext}$	
External magnetic field magnitude	B^{ext} = 0.0575 T
Geomagnetic field (coordinates – Riga, Latvia)	B^{Earth} = 0.00005 T
***Lorentz* force magnitude** – current interaction with:	
self-magnetic field – $max\|\boldsymbol{f}^{self}\|$	$7.35 \cdot 10^4\ N/m^3$
external magnetic field – $max\|\boldsymbol{f}^{ext}\|$	$5.45 \cdot 10^4\ N/m^3$
geomagnetic field – $max\|\boldsymbol{f}^{Earth}\|$	$5.47 \cdot 10\ N/m^3$
Total Lorentz force – $max\|\boldsymbol{f}^{total}\|$	$8.92 \cdot 10^4\ N/m^3$

A. Structure of EVF

Maximum value of the *Lorentz* force (Table III), determined in (1), is reached in immediate proximity to the top electrode where the force distribution is almost axis-symmetrical (Fig. 3a). The velocity field is almost axis-symmetrical not only in the melt mirror zone, but also in bottom zone (Fig. 2a) despite of *Lorentz* force symmetry about each of the two bottom electrodes. Streamlines indicates dominating toroidal vortex (Fig. 3a) with jet direction from the top electrode to the bottom zone. There are also two small vortices in peripheral zone near side wall that are similar to the patterns discussed in [5, Fig. 9a] and [6, Fig. 12].

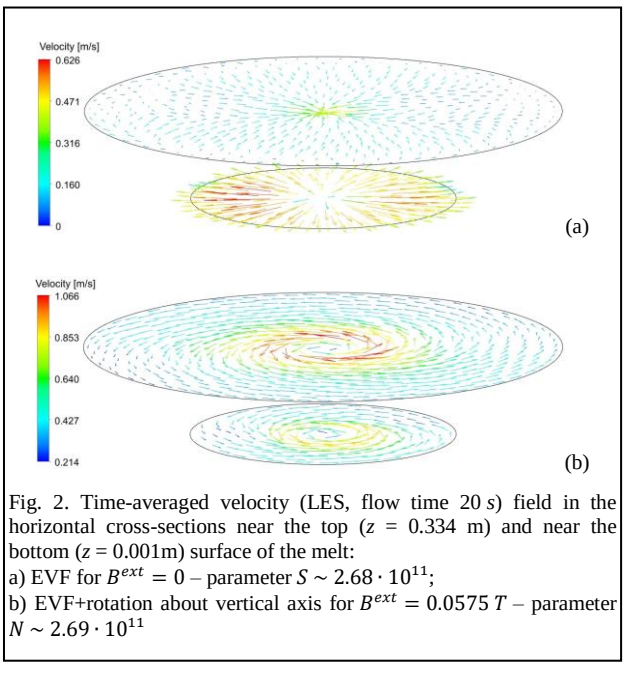

Fig. 2. Time-averaged velocity (LES, flow time 20 *s*) field in the horizontal cross-sections near the top (z = 0.334 m) and near the bottom (z = 0.001m) surface of the melt:
a) EVF for $B^{ext} = 0$ – parameter $S \sim 2.68 \cdot 10^{11}$;
b) EVF+rotation about vertical axis for $B^{ext} = 0.0575\ T$ – parameter $N \sim 2.69 \cdot 10^{11}$

B. Melt rotation in external magnetic field

If magnetic field $\boldsymbol{B}^{ext}$ is of the same order with the self-magnetic field $\boldsymbol{B}^{self}$ (Table III) and $S \sim N \sim 2.7 \cdot 10^{11}$ (4), the *Lorentz* force (2) has a strong azimuthal component (Fig. 3b) that drives rotation in the melt mirror zone about the top electrode axis (Fig. 2b). The rotation is counter clock-wise in the case of external axial magnetic field with upward direction (Fig. 1).

C. Influence of geomagnetic field

The maximum value of contribution to *Lorentz* force due to interaction of electrical current with geomagnetic field $\boldsymbol{f}^{Earth} = \boldsymbol{j} \times \boldsymbol{B}^{Earth}$ is three orders of magnitude smaller than the result (1) of electrical current interaction with the self-magnetic field – $max|\boldsymbol{f}^{Earth}| \ll max|\boldsymbol{f}^{self}|$ (Table III). Similarly parameter N is three orders smaller – $N \sim 2.4 \cdot 10^8$ (compare with value in previous section *B*). Thus the geomagnetic field does not affect EVF in the considered DC EAF of industrial scale.

Note, that in the case when *Lorentz* force $\boldsymbol{f}^{\text{self}}$ (1) is artificially "switched off" the rotation is clock-wise because geomagnetic field has downward direction.

References

[1] S. Pavlovs, A. Jakovics, E. Baake, and B. Nacke, "Melt flow patterns in metallurgical MHD devices with combined inductive and conductive power supply," Magnetohydrodynamics, vol. 50, pp. 303–316, 2014.

[2] A. Chudnovsky, Yu. Ivochkin, A. Jakovics, I. Teplyakov, S. Pavlov and D. Vinogradov, "Investigations of electrovortex flows with multi electrodes power supply," Magnetohydrodynamics, vol. 56, pp. 487–498, 2020.

[3] S. Pavlovs and A. Jakovics, "Comparison of experimental and numerical velocity for electrovortex flow in multi-electrode furnace", International Symposium on Heating by Electromagnetic Sources, Padua, Italy, pp. 143–148, May, 2019.

[4] S. B. Dement'ev, A. I. Chaikovskii and A. Yu. Chudnovskii, "Generation of electrovortex flows in liquid-metal baths with a multielectrode current input," Magnetohydrodynamics, vol. 24, pp. 76–80, 1988.

[5] S.A. Smirnov, V.V. Kalaev, S.M. Hekhamin, M.M. Krutyanskii, S.N. Kolgatin, and I.S. Nekhamin, "Mathematical simulation of electromagnetic stirring of liquid steel in a DC arc furnace," High Temperature, vol. 48, pp. 68–76, 2010.

[6] A. Chudnovsky, "Physical modelling of 3D melts mixing for electrometallurgical aggregates," Magnetohydrodynamics, vol. 53, pp. 747–758, 2017.

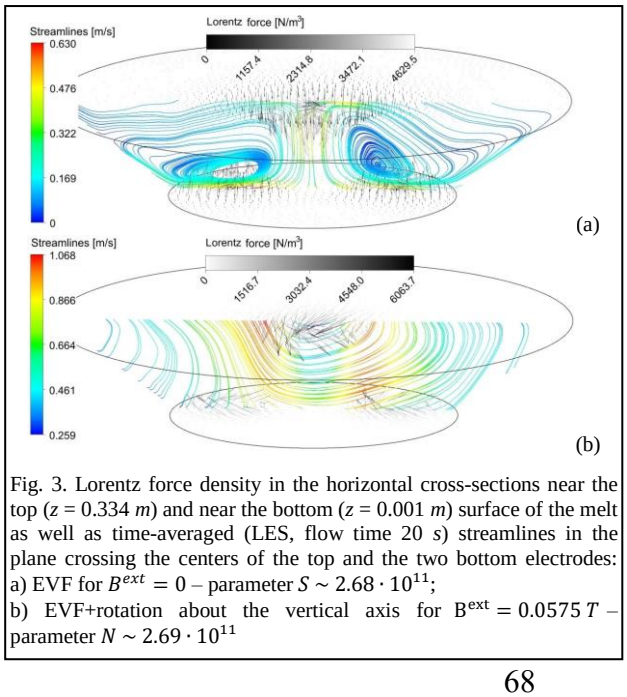

Fig. 3. Lorentz force density in the horizontal cross-sections near the top (z = 0.334 *m*) and near the bottom (z = 0.001 *m*) surface of the melt as well as time-averaged (LES, flow time 20 *s*) streamlines in the plane crossing the centers of the top and the two bottom electrodes:
a) EVF for $B^{ext} = 0$ – parameter $S \sim 2.68 \cdot 10^{11}$;
b) EVF+rotation about the vertical axis for $B^{ext} = 0.0575\ T$ – parameter $N \sim 2.69 \cdot 10^{11}$